IBRO Reports 3 (2017) 45–54

Contents lists available at ScienceDirect

IBRO Reports

journal homepage: http://www.journals.elsevier.com/ibro-reports

Research Paper

Xenon pressure dependence on the synchronized burst inhibition of rat cortical neuronal network cultured on multi-electrode arrays

Tsutomu Uchida*, Koichiro Shimada, Ryutaro Tanabe, Tatsuya Kubota, Daisuke Ito, Kenji Yamazaki, Kazutoshi Gohara

Division of Applied Physics, Faculty of Engineering, Hokkaido University, N13 W8 Kita-ku, Sapporo, Hokkaido 062-8628, Japan

ARTICLE INFO

Article history:
Received 15 May 2017
Received in revised form 4 August 2017
Accepted 1 September 2017

Keywords:
Xenon
Oxygen
Partial pressure
General anesthesia
Multi-electrode array
Synchronized burst

ABSTRACT

Mature rat cortical neuronal networks cultured on multi-electrode arrays (MEAs) are known to show spontaneous synchronized bursts accompanied by independent single spikes. The spontaneous synchronized bursts can be inhibited by Xe gas. In this study, we adjust the Xe gas pressure to control the amount of Xe in a neuron-cultured MEA medium. We show that the synchronized bursts cease completely within several minutes by applying Xe gas at partial pressures above 0.3 MPa. After depressurizing and purging with fresh air, the synchronized bursts recover to their original frequency. Thus, we confirmed that Xe acts as a network-activity inhibitor of the cultured neuronal network on MEAs. But below 0.3 MPa, the synchronized bursts are inhibited only partially, depending on the Xe partial pressure. Based on the partial-pressure influence on the change of the neuronal network activities, we find the critical concentration of Xe for the inhibition effect to be approximately 9.5 mM, a value above which more than 90% of the synchronized burst activity is inhibited. Further systematic observations with Xe-air mixed gases show that pressurized air with a small amount of Xe suppresses the inhibition of synchronized bursts, suggesting an air component that can accelerate the synchronized bursts.

Introduction

General anesthesia is a physiological state characterized by loss of consciousness, loss of sensation through analgesic effects, immobilization, and temporary amnesia (Stedman's Medical Dictionary, 2006). These physiological effects are thought to be caused by a depressant effect on the central nervous system from the anesthetic agent. However, for anesthetic agents in the gaseous state, such as xenon (Xe), the specific molecular mechanisms by which they operate remain unclear. Despite the uncertain mechanism, however, Xe is expected to be useful clinically as a general anesthetic without causing undesirable side effects (Preckel and Schlack, 2005).

The narcotic effect of Xe was first reported on mice (Lawrence et al., 1946) and later on humans (Cullen and Gross, 1951). The effect was attributed to Xe's high fat solubility and high oil/water coefficient, and following the Meyer-Overton correlation, thought to act *via* the lipid-dissolution hypothesis (Meyer, 1899; Mayer, 1937; Overton, 1901). Although the Mayer-Overton correlation is not accepted as the main mechanism for general anesthesia, a sufficient amount of Xe dissolves into both the lipid bilayer (Booker and Sum, 2013) and into the multi-layered liposomes (Uchida et al., 2015) to have some effects on the electric activities of neurons.

As an alternative mechanism for general anesthesia, Pauling and Miller independently proposed the clathrate hypothesis in which the electrical signals are inhibited by a clathrate hydrate at synapses (Pauling, 1961; Miller, 1961). This hypothesis is opposed by several researchers (*e.g.*, (Dawe et al., 1964; Miller, 1969)) because the physiological condition is far from that needed for clathrates to form. However, it has received supports from theoretical (Dorsch, 1970; Dorsch and deRocco, 1973), experimental (Schoenborn et al., 1964; Dorsch and Distefano, 1973), and clinical (Matsumoto, 1995) investigations.

At the end of the 20th century, the focus shifted to mechanisms involving direct protein interactions. Several pharmacological studies with the patch-clamp method, which provides single channel- and whole-cell-level responses of a single neuron, suggest that inhalation anesthetics such as Xe affect the configuration change of channel proteins in the plasma membrane (Evers et al., 1987; Nakahiro et al., 1989). However, Xe is a monatomic and noble gas, which is essentially inert. Unlike the more commonly used

* Corresponding author.
E-mail address: t-uchida@eng.hokudai.ac.jp (T. Uchida).

https://doi.org/10.1016/j.ibror.2017.09.001

general-anesthetic gases, such as isoflurane, Xe was found to have no significant effect on either the inhibitory postsynaptic currents by γ-aminobutyric acid (GABA) or on currents evoked by exogenous application of GABA in cultured neurons (Franks et al., 1998; de Sousa et al., 2000; Georgiev et al., 2010).

But there are other possible pathways for Xe to affect the electric activities of neurons. For example, Xe acts as an antagonist of glutamatergic receptors, with inhibition of *N*-methyl-D-aspartate (NMDA) receptors being the mechanism implicated most often (Franks et al., 1998; de Sousa et al., 2000; Ma et al., 2002). Also, computer simulations identify several potential action sites of Xe in the ligand-binding domain of an NMDA receptor (Dickinson et al., 2007; Liu et al., 2010 Liu et al., 2010). However, results with glutamatergic receptors have been inconsistent, with some studies showing that Xe acts on non-NMDA glutamatergic receptors of *C. elegans*, rather than NMDA receptors (Negale et al., 2005), and some showing that Xe acts on both receptors (Dinse et al., 2005; Haseneder et al., 2008). Furthermore, recent studies have indicated that NMDA receptors do not mediate the immobility effects of Xe and other inhaled anesthetics (Eger et al., 2006, 2008). As another pathway, Xe has been shown to affect nicotinic acetylcholine receptors (Yamakura and Harris, 2000) and certain potassium channels (Gruss et al., 2004). These inconsistencies of the *in vivo* interactions between Xe and receptors have also been reported from the whole-brain level responses *via* position emission tomography studies (Kaisti et al., 2003; Rex et al., 2006; Laitio et al., 2007, 2009; Salmi et al., 2008). To explain these varied results, the 'pocket hypothesis' advocated by Franks and Lieb (1994) has been accepted as the mechanism of Xe-inducing general anesthesia (Hirota and Sasaki, 2011). This concept assumes that the proteins on the cell membrane have the molecular architecture of a binding site for Xe.

To study the Xe-induced narcotic effect of such a nerve system at the mesoscopic scale (between single-neuron and tissue scale), multi-electrode arrays (MEAs) can provide a good *in vitro* model. For instance, Ito et al. (2010) studied the electric activity development by both MEA measurements and immunofluorescent staining observations. They clearly showed that the electric activities of neuronal networks changed from random-spontaneous firing to the synchronized bursts (SBs). Later, by applying a gas pressure system to a neuronal network on a MEA, Uchida et al. (2012) found that the spontaneous SBs of a mature neuronal network was completely inhibited by applying 0.3 MPa Xe, whereas single spikes remained. The inhibited SBs later recovered after depressurization of the Xe gas. Moreover, as the retaining of single spikes during the suspension of SB did not fit the lipid-dissolution hypothesis, Uchida et al. (2012) considered that the suspension was due to inhibition of the synapse transmission by the dissolved Xe.

As the amount of dissolved Xe depends on the partial pressure (*e.g.*, *via* Henry's law), the Xe-induced SB inhibition should be controlled by the external Xe pressure. In the present study, we examine the pressure dependence of Xe gas on the inhibition of SB in a mature rat cortical neuronal network on a MEA. We ask what pressure of Xe is needed to completely inhibit SB, and how does air and its constituents affect this inhibition?

Briefly, we find here that Xe inhibits the spontaneous SBs in the neuronal network at a partial pressure even below 0.3 MPa, with the inhibition becoming complete above 0.3 MPa (total pressure of 0.4 MPa). Based on the Hill equation fitting for the partial pressure dependence on the SB inhibition, this critical pressure corresponds to the Xe concentration of about 10 mM, which coincides well with the minimum alveolar concentration for a rat. Under pressures of pure air, or a small amount of Xe including air, however, we found an acceleration effect on SBs. As adding nitrogen (N_2) gas or a mixture of air and 5% carbon dioxide (CO_2) has little discernible effect on inhibition, we suggest that oxygen (O_2) accelerates the SB. Therefore, we conclude that the degree of SB inhibition in the Xe-air mixture gas under pressure involves competing effects between Xe-induced SB inhibition and O_2-induced SB acceleration.

Experimental procedures

The sample preparation and the experimental setup are practically the same as those in Uchida et al. (2012), so here we give only a brief description. We start with commercially available dissociated cortex prepared from Wistar rats at embryonic day 17 (Nerve-Cell Culture System; Sumitomo Bakelite, Tokyo, Japan). The dissociated cells are plated with a nominal density of 5000 cells/mm^2 onto a MEA (multi-electrode dish (MED) probe: Alpha MED Scientific, Osaka, Japan). This MEA consists of 64 poly(ethylenimine)-coated microelectrodes in an 8×8 array plus 4 reference electrodes (Ito et al., 2010; Uchida et al., 2012; Kudoh et al., 2007; Hosokawa et al., 2008) at the bottom of a glass dish (22-mm inner diameter × 10-mm height). The plated neurons are cultured in Neuron Culture Medium (Sumitomo Bakelite), which is serum-free conditioned medium from 48-h rat astrocyte-confluent cultures, based on Dulbecco's modified Eagle's minimum essential medium (DMEM)/F-12 with N2 supplement (Banno et al., 2005; Takeuchi et al., 2005).

Each microelectrode is $50 \times 50\ \mu m^2$ with a spacing of 150 μm. To avoid cell attachment onto reference electrodes, we use a cloning ring with an inner diameter of 5 mm and a total area of 19.6 mm^2 (Honma et al., 1998). The rings are removed after adhesion of the dissociated neurons on the MED probe (approximately 3 hours). The firing activity of each culture is recorded at a sampling rate of 20 kHz using a MED64 extracellular recording system (Alpha MED Scientific), with the MED64 conductor software used for the A/D conversion.

The cultures are incubated at 310 K in the Neuron Culture Medium in humidified air containing 5% CO_2. After 3 days in the Neuron Culture Medium, a half of the medium is replaced with fresh DMEM/serum medium. This medium-replacement procedure is done twice a week for several weeks. The DMEM/serum medium consists of DMEM (Life Technologies-Gibco, or ThermoFisher-Gibco, Waltham, MA, USA; hereafter, ThermoFisher-Gibco) supplemented with 5% fetal bovine serum (ThermoFisher-Gibco), 5% horse serum (Sigma-Aldrich, St. Louis, MO, USA), 25 μg/mL insulin (ThermoFisher-Gibco), 100 U/mL penicillin, and 100 μg/mL streptomycin (ThermoFisher-Gibco) (Ito et al., 2010). Thus, the Neuron Culture Medium is gradually replaced with the DMEM/serum medium during culture. The adhesion and growth of cultured neurons are observed under a phase-contrast microscope (Olympus, Tokyo, Japan; type CKX-41). The electric activity enhancements of the cultures are checked *via* 5-min recordings with the MED64 extracellular recording system. Then, between 15 and 25 days *in vitro* (DIV), the mature samples are used in the gas-pressurizing experiments.

To measure the electric activities of neuronal networks under high pressures, we used a high-pressure vessel equipped with the MED connector (Taiatsu Techno, Tokyo, Japan). The vessel is installed in an incubator to maintain a sample temperature of 310 ± 1 K. Due to the limitation of the vessel, we can record only the 16 electrodes at the center of the MED probe. The pressure and temperature in the vessel are monitored by a pressure transducer (Yokogawa, Tokyo, Japan; type FP201-C22-C20A*B) and a type-T thermocouple and recorded by a data logger (Grapthec, Yokohama, Japan; type GL400). The optical monitoring system allows us to observe the change of cell morphologies during the experiments.

The experimental procedure has four periods: (I) A 1-hr control period involving pre-pressurization measurements of the firing activities at 310 ± 1 K and atmospheric pressure with normal air. This period also aims to stabilize the electric activities of the sample, which are disturbed during the sample set-up. We consider

the electric activities during the last 10-min of this period to be the sample's control condition. (II) A 1-hr pressurizing period, in which Xe gas (purity of 99.995%; Air-Water, Wakayama, Japan) or Xe-air mixed gas is introduced to the vessel at the experimental pressures. The mixed gas is prepared by mixing Xe gas with pressurized air (dried air; Hokkaido Air-Water, Sapporo, Japan). We avoided purging the initial air with Xe, so we distinguish the total pressure P from the partial pressure P_{Xe} of Xe. (III) A 1-hr depressurization period, in which the pressure is reduced to an atmosphere over several minutes by releasing gas from the high-pressure vessel. (IV) A 1-hr purge period, in which purged gas (dried air) flows for several minutes to flush Xe out of the vessel. After finishing these measurements, we return the MED probe to the cultivation incubator to check for damages to the pressured sample. Damages are checked by observing the morphologies and measuring the firing activities for several days after the experiment.

The detection procedures and criteria for spikes and synchronized bursts are the same as those in Ito et al. (2010) and Uchida et al. (2012). Briefly, a spike is identified when the intensity of the extracellular potential exceeds a threshold within a window of 1 ms. To determine this threshold, we apply the method in Ito et al. (2010) in which we first evaluate the level of biological and thermal noises (usually 10–20 μV) over the complete dataset for the experiment. The value of the threshold is determined for every 5-min of data broken up into successive segments, which varies even in an experimental run (approximately from −10 to −50 μV). We then use the tangent method on the peaks that exceed this level. Then we plot the single spikes and synchronized bursts in a spike raster-plot, and count the spike rate (SR) and synchronized-burst rate (SBR). This is done over the 15 electrodes in the center of the probe (area of $650 \times 650\ \mu m^2$). A burst is defined here as a time period with spike density exceeding 7 per 100 ms, a period that terminates at a density that lies below the threshold for at least 300 ms. A synchronized burst is said to occur when at least three channels record the burst signal simultaneously.

For analyses of SR and SBR, we use a total activity per minute averaged over 5 min to smooth the fluctuation of neuronal network activities. To compare the different experimental runs, we employ the scaled SBR (s-SBR), in which each 5-min-averaged SBR is normalized by the average SBR value of the steady-state condition. About this condition, we found that the firing activities always stabilized before 50 min had elapsed. Thus, we assume that steady-state occurs during the last 10 min of the 60-min control period. This normalization procedure avoids the artifacts due to data fluctuations in the early stage of the control period, which can vary by sample.

For the P dependence experiments, Xe gas is added from 0.1 to 0.5 MPa to the normal air condition, which results in a P range from 0.2 to 0.6 MPa. We repeat this experiment several times on different cultures to establish a reproducible P dependence ($n = 8, 4, 9, 2$, and 4 for $P = 0.2$, 0.3, 0.4, 0.5, and 0.6 MPa, respectively). The data obtained in the present study is averaged at the indicated experimental conditions ± the standard deviation (SD) of all measured data. Then, data are analyzed by one-way ANOVA with a Tukey-Kramer post-hoc test (Microsoft Excel 2010 and BellCurve for Excel) for at least 99% confidence ($p < 0.01$). For the P_{Xe} dependence experiments, on the other hand, we aim to obtain the qualitative trend of the SB inhibition depending on P_{Xe} in wider experimental conditions. So, we ran the Xe + air (dried air) mixed gas pressurization tests at $P_{Xe} = 0$–0.4 MPa for P ranging between 0.2 and 0.5 MPa. Thus, the P-dependence runs include only one or two trials, and hence we show the qualitative results without statistical analysis. For examining the acceleration effect of air on the SBs, we use pure N_2 (purity of 99.999%, Hokkaido Air Water, Hokkaido, Japan) or air with 5% CO_2 (dried air base 5% CO_2; Hokkaido Air Water) instead of Xe gas.

To examine the network growth, we take several samples and stain the neurons after the pressurizing experiment. For the staining, the primary antibodies are anti-MAP2 (microtubule-associated protein 2) mouse IgG (1:500; Sigma-Aldrich) and anti-NF200 (neurofilament 200 kD) rabbit IgG (1:1000; Sigma-Aldrich). The secondary antibodies are Alexa Fluor 488 goat anti-rabbit IgG (Life Technologies-Molecular Probes) and Alexa Fluor 546 goat anti-mouse IgG. Cell nuclei are stained with Hoechst33342 (Wako Pure Chemical Industries, Osaka, Japan). See Ito et al. (2010, 2013) for the staining procedures. The culture after the pressurization test on a MEA is fixed with 4% formaldehyde in phosphate-buffered saline (PBS; ThermoFisher-Gibco) solution for 10 min. After permeabilization with 0.5% Triton X-100 (Sigma-Aldrich) in PBS solution for 10 min, the culture is incubated with PBS solution containing 10% goat serum (ThermoFisher-Gibco) and 0.01% Triton X-100 for 30 min. The permeabilized culture is incubated with primary antibodies in PBS solution containing 10% goat serum overnight at 277 K and then rinsed with PBS solution for 10 min three times. The culture is then incubated with secondary antibodies (0.4% in PBS solution containing 10% goat serum) for 1 h at room temperature and rinsed three additional times. To observe the cell nuclei, the culture is incubated with 1 μg/mL Hoechst33342 for 10 min after incubation with secondary antibodies. Fluorescence images are captured using an epifluorescence microscope (Olympus; type IX71) through a 20 × objective (Olympus; type LCPLFL 20 ×) and collected with a charge-coupled device camera (Olympus; type DP70).

Results

Neuronal network activity changes

The dispersed rat cortical neurons cultivated on a MED probe spread and adhered on both the glass plate and electrodes (*e.g.*, Fig. 1a). During the cultivation of neurons, the growth of the neuronal network is observed through a microscope and monitored *via* the spike measurements. About one week after plating, neurons started firing spontaneously, and then the spikes synchronized between different channels. At that moment, some neurons are connecting and forming a network. After the network formed, the firing signals also started producing bursts. The bursts then synchronized as the network grows further, with the synchronized burst rate (SBR) becoming constant after two or three weeks after plating. We confirm that the neuronal network consists of axons and dendrites by inspection (*e.g.*, Fig. 1b and c), then use such mature neuronal network samples for the Xe-pressure test.

Here we show a typical change of electric activities of the neuronal network during the Xe-pressure test. Fig. 2 shows a snapshot of the MEA signals and corresponding spike raster plots at $P_{Xe} = 0.5$ MPa ($P = 0.6$ MPa). (See Fig. S1 for the corresponding time series of the spike rate N_0 and SBR.) These plots indicate that spontaneous SBs occur in 14/15 channels (93%), and that most of the spikes are included in each SB. (We cannot detect any signals on #13 channel due to the present experimental set-up.) The spontaneous single spikes occur on only a few electrodes (*i.e.*, #4, #14, and #15 in this sample). SR and SBR are a little scattered early in the control period due to the experimental disturbance, but they gradually recover and reach a constant value at approximately 6×10^3 cpm (counts per minute) and 22 cpm, respectively. These variations are within the range of the variations usually observed during normal cultivation for several weeks (*e.g.*, Ito et al., 2010).

After applying Xe pressure, no experiment showed any morphological changes as viewed with an optical microscope. Based on the color of the medium, which includes phenol red, we consider that the observed change of pH during the experiment was

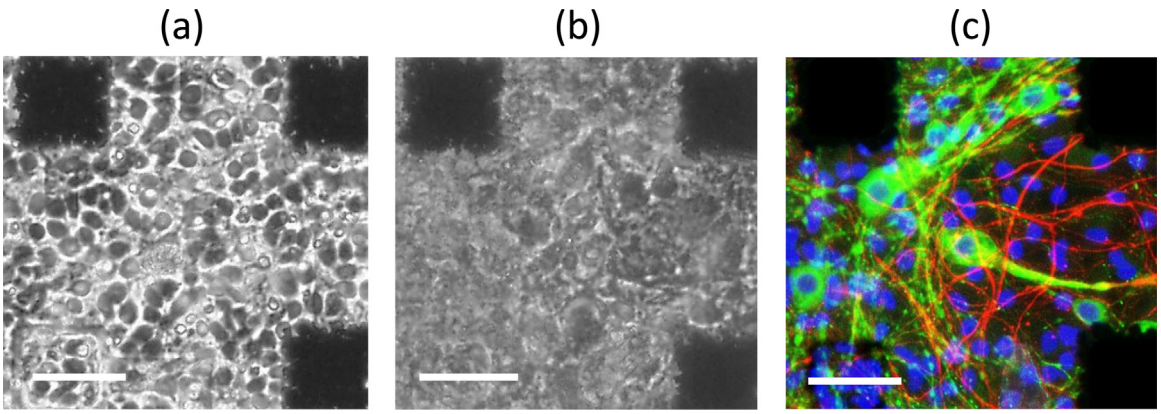

Fig. 1. Microscopic image of neurons cultured on an MEA. The black squares (microelectrodes) in each corner are 50 μm on each side. Each scale bar shows 50 μm. (a) Neurons after seeding. (b) Mature neuronal network at 26 DIV (before experiment). (c) Immunofluorescence image of neuronal network just after the experiment (red: NF200, green: MAP2, and blue: nuclei).

not large enough to affect the nerve activities. However, the electric activities clearly change. Comparing Fig. 2(I) and (II), notice that SBs vanish in (II) yet some single spikes remain (#14 and #15 in Fig. 2(II)). We sometimes observed that some electrodes recorded a frequent firing after vanishing SBs, such as that shown at #7 and #8 in Fig. 2(II). As shown in Fig. S1, the inhibition of SBs occurs soon after Xe pressurization, and becomes almost complete within 20 min after pressurization (t = 60–80 min).

The observed electric activity inhibition under Xe pressure starts to recover after depressurization (t > 120 min in Fig. S1). As shown in Figs. 2 (III), (IV), and S1, a few bursts recover after depressurization and then synchronize, resulting in SBR gradually increasing with slight scattering. Simultaneously, the frequent firing observed during SB inhibition (as shown at #7 and #8 in Fig. 2(II)) become gradually quiet (Fig. 2(III)).

After purging the remaining gas with air (t > 180 min in Fig. S1) in period IV, the SB recovers to its previous high frequency in period I. However, the burst pattern does not recover immediately, but gradually approaches that of the period I (compare Fig. 2(I) and (IV)).

To compare these detailed signal changes with the macroscopic neuronal network activity changes, we show in Fig. 3 the time series of s-SBRs under various P conditions from 0.2 to 0.6 MPa. This figure shows that the inhibition-recovery processes of SBs with Xe pressure mentioned in Figs. 2 and S1 are qualitatively coincident in all P conditions. This is also consistent with the results obtained in our previous study (Uchida et al., 2012). Therefore, we consider that the Xe-induced inhibition mechanism should be the same within our experimental conditions. We now examine the pressure dependence on the SB inhibition.

Xe pressure dependence on the synchronized burst inhibition

From Henry's law, the Xe concentration in the medium (C_{Xe}) is larger under higher P_{Xe}. To investigate, we added a Xe pressure P_{Xe} of 0.1–0.5 MPa to an atmosphere of air, making a total pressure P that ranged from 0.2 to 0.6 MPa. The time series of s-SBR under Xe pressure (period II in Fig. 3) shows that SB becomes suppressed immediately after Xe-pressurization. Then, the s-SBR of each P condition reaches its stable value within 20-min after pressurization (t > 80 min in Fig. 3). The average of each stable value is shown by the dashed line in Fig. 3(II).

When P equals or exceeds 0.4 MPa, s-SRB reaches to zero within 20 min of Xe pressurization. Specifically, at P = 0.6 MPa (n = 4), s-SBR becomes zero after 8.0 ± 2.1 min, but the time is 16.5 ± 4.9 min at P = 0.5 MPa (n = 2) and 12.2 ± 14.8 min at P = 0.4 MPa (n = 9). The SBs are completely inhibited until the end of the pressurizing period II under these conditions. On the other hand, when P < 0.4 MPa, a small number of SBs remain even at t > 80 min as shown in dashed lines in Fig. 3. To evaluate the pressure effect on the SB inhibition, we determine the inhibition effect of SBs Δ as

$$\Delta = (\text{averages-SBRat} t = 80\text{–}120\,\text{min})/(\text{averages-SBRat} t = 50\text{–}60\,\text{min}), \quad (1)$$

where the numerator is the steady-state s-SBR under the Xe-induced inhibition condition (from 20-min after pressurization to the end of period II) and the denominator is the standard s-SBR in the last 10-min of the period I. Then we obtained Δ values under various P_{Xe} in Fig. 4. Based on the Tukey-Kramer test, both Δ = 0.15 ± 0.02 at P_{Xe} = 0.2 MPa (n = 4) and Δ = 0.48 ± 0.05 at P_{Xe} = 0.1 MPa (n = 8) are significantly larger than those observed at P_{Xe} larger than 0.3 MPa (p < 0.01). This figure clearly shows that the degree of SB inhibition depends on P_{Xe}, and the threshold for complete inhibition occurs at P_{Xe} approximately equal to 0.3 MPa. This value is consistent with the result obtained in our previous work (Uchida et al., 2012).

Xe-partial pressure dependence on the synchronized burst inhibition

We then examined the influence of total pressure P on the SB inhibition effect by running similar experiments under various P_{Xe} conditions. For these experiments, P_{Xe} ranges from 0.1 to 0.4 MPa by pressurizing with a Xe-air mixture. Although the total pressure changed in these experiments, the partial pressures of the other air components, including oxygen, remained fixed. To obtain the inhibition trend on SBs qualitatively, we ran one or two experiments for each P-P_{Xe} condition and examined them under finer experimental conditions.

Fig. 5a–d shows the resulting Δ dependence on P_{Xe} under various P conditions. (For a time-series of s-SBR in pressurizing period II at various P, see Fig. S2a–d.) Values of Δ from Fig. 4 (*i.e.*, 1 atmosphere of air) are also plotted in this figure by solid marks with error bars. These figures show that Δ decreases when P_{Xe} increases, and that Δ vanishes at P_{Xe} larger than 0.3 MPa, although this critical P_{Xe} value seems to depend slightly on P. It is interesting, on the other hand, that Δ values exceed unity under low P_{Xe} conditions (especially P_{Xe} < 0.1 MPa). This means that the spontaneous SBs under air-pressurizing conditions are accelerated, and thus the SBs are affected by both a Xe-induced inhibition and an air-induced acceleration under lower P_{Xe} conditions (0 < P_{Xe} < 0.2 MPa).

As the acceleration effect of air tends to be large at large P when P_{Xe} = 0 MPa (in Fig. 5), it appears that some air components may accelerate the neuronal network activities. To check the activ-

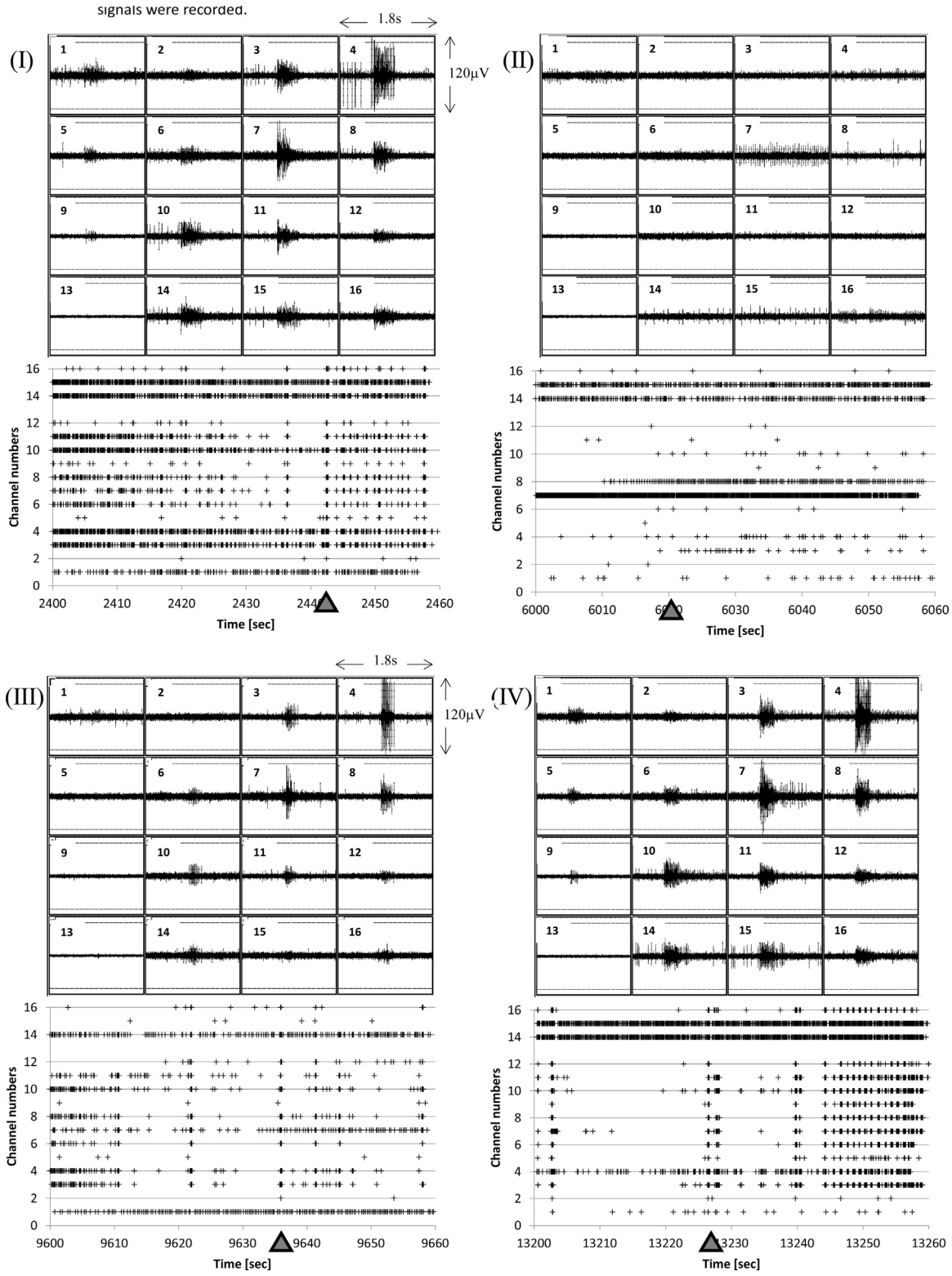

Fig. 2. MEA signals of every channel (top) and their spike raster plots (bottom). (I) At 40-min into the control process. (II) At 40-min after Xe pressure introduced at P_{Xe} = 0.5 MPa. (III) At 40-min after depressurization. (IV) At 55-min after purge by air. #13 is the reference channel (no signal was detected). Triangles in the spike raster plots show the time when the above MEA signals were recorded.

ity change with the kind of gas, we ran similar experiments with pure N_2 gas and with the air having 5% CO_2, with a total pressure P = 0.4 MPa in all cases. The time series of s-SBR of these experiments in the pressurizing period II are shown in Fig. 6. These results indicate that the Δ values for both N_2 and CO_2 have no acceleration effect on the SB activities, in contrast to those for air (no Xe). Therefore, the acceleration effect on SBs appears to be due to the increase of P_{O2}, the partial pressure of oxygen (O_2).

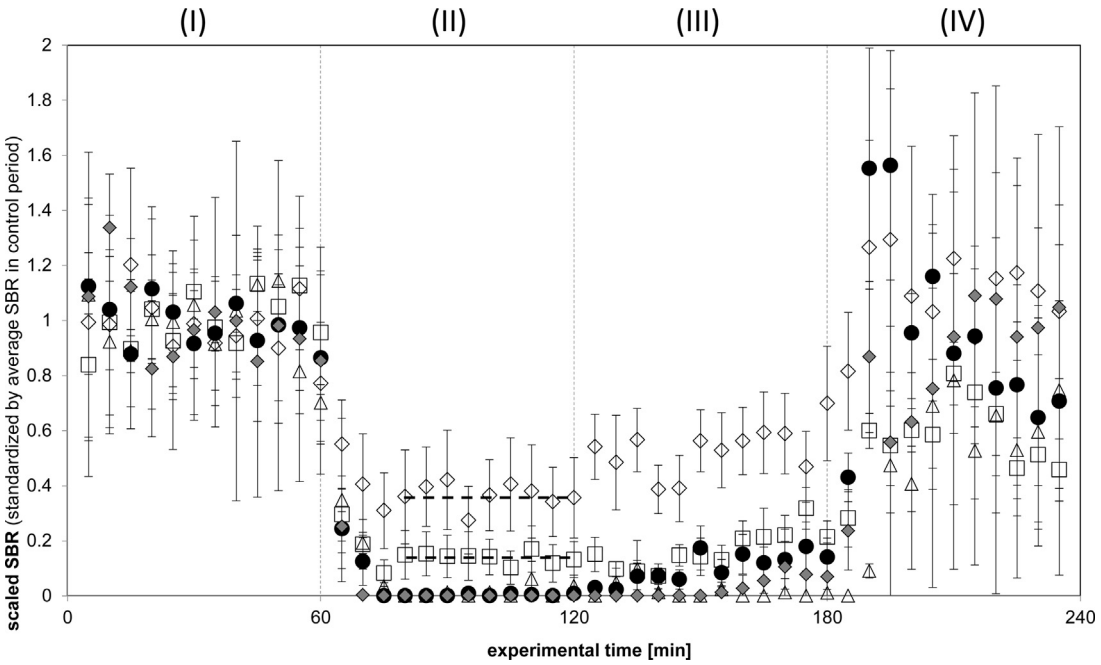

Fig. 3. Scaled synchronized burst rate (s-SBR) variations in the P dependence experiments (P = 0.2 MPa: open diamond (n = 8), 0.3 MPa: open square (n = 4), 0.4 MPa: solid circle (n = 9), 0.5 MPa: open triangle (n = 2) and 0.6 MPa: solid diamond (n = 4)). Values are scaled SBR with running 5-min averages. Error bars shows the standard deviations (±SD) from the different experiments. The periods are t = 0–60 min: control (period I), t = 60–120 min: pressurized (period II), t = 120–180 min: depressurized (period III), t = 180–240 min: flushed with air (period IV). Dashed lines in period II show the average value at t = 80–120 min for P = 0.2 MPa and 0.3 MPa, both of which are sufficiently different from those for P = 0.4 MPa and higher ($p < 0.01$).

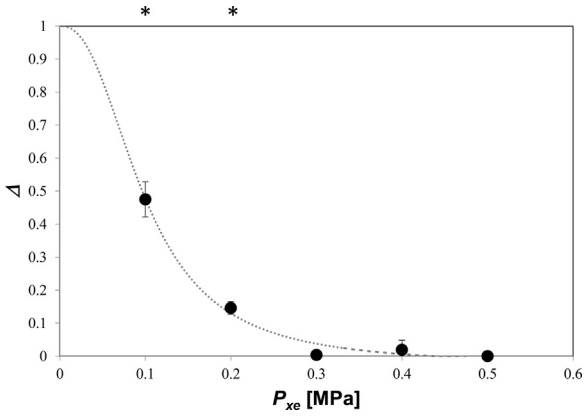

Fig. 4. The inhibition effect Δ for various partial Xe pressures P_{Xe}. Error bars shows the standard deviations (±SD) from the different experiments. The number of experiments n is 8, 4, 9, 2, and 4 for P = 0.2, 0.3, 0.4, 0.5, and 0.6 MPa conditions, respectively. The asterisks mark cases with a significant difference of Δ compared to the large suppression at higher P_{Xe} ($p < 0.01$ by Tukey-Kramer test). The dotted line is the fit from the Hill equation.

Discussion

SB inhibition of neuronal network activities after Xe pressurization

A spontaneous burst in an *in vitro* neuronal network occurs when a sufficient number of neurons connect into a neuronal network, each connection being mainly *via* synaptic junctions (Ito et al., 2010, 2013). The SBR increases with an increasing number of neurons connected in the network, and also increases with the number of synaptic junctions (Wilson et al., 2007). Therefore, SBR is an index of the neuronal network maturation.

In the present study, the spontaneous SBs in mature neuronal networks are observed to decrease soon after the Xe pressurization, a finding consistent with our previous study (Uchida et al., 2012). We also observed that the depression of SBs became constant within 20-min after pressurization. Here we discuss this rate of inhibition. Based on the concept of anesthetic gas dissolved into the blood, we consider that the activity-change rate after gas pressurization depends on factors (a) the amount of Xe reaching the neuronal network, (b) the number of active sites inhibited by Xe, and (c) the time constant of the SB-inhibition process. These factors may also apply to the apparent O_2-induced acceleration effect.

Factor (a) should be related to the dissolution of Xe from the gas into liquid by pressurization, followed by diffusion to the bottom of the MEA dish, driven by the Xe concentration gradient. As the solubility of a gas depends on its partial pressure, P_{Xe} is an important parameter to control the activity-change rates. After Xe dissolves into the medium, it builds up at the bottom of the MEA dish near the mature neuronal network and reacts with neurons, a reaction that modifies the electric activities of the network. The rate of this reaction should depend on factors (b) and (c) above. As both the initial number concentration of neurons (5000 cells/mm^2) and the maturation procedure are about the same in every experiment, we argue that the connections between neurons in the neuronal network are similar (Ito et al., 2013), meaning that factor (b) is about the same for all samples.

For the present experimental conditions, we can assume that the amount of dissolved gas obeys Henry's law. Designate the initial concentration of gas i (i = Xe or O_2) at the liquid surface as c_{0i}. Thus, c_{0i} depends on the partial pressure P_i. From the liquid surface, these components diffuse in the culture medium, driven by their concentration gradient towards the bottom of the MEA dish. This diffusion path is essentially one-dimensional given that the gas/liquid interface width (~22-mm diameter) is much larger than the depth (~4 mm). Thus, we assume one-dimensional diffusion to depth z, neglecting convection. Then, the relevant diffusion equation is

$$dc_i/dt = D_i d^2c_i/dz^2, \quad (2)$$

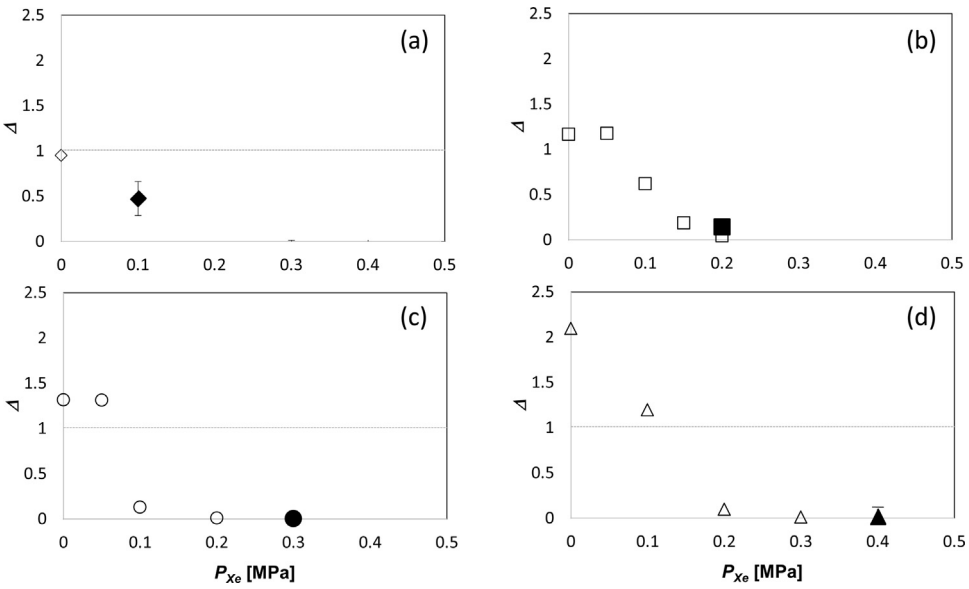

Fig. 5. The inhibition effect Δ for a range of partial Xe pressures P_{Xe} in air-Xe mixed gases of various total pressures P. (a) P = 0.2 MPa. (b) P = 0.3 MPa. (c) P = 0.4 MPa. (d) P = 0.5 MPa. Open marks are obtained in P_{Xe} dependence experiments. As each mark is obtained by just one or two experiments, no error bars are shown. Solid marks are obtained in the P-dependence experiments (shown in Fig. 4), for which error bars show the standard deviations. Dotted line shows Δ = 1, above which s-SBR is accelerated during the pressurizing period II.

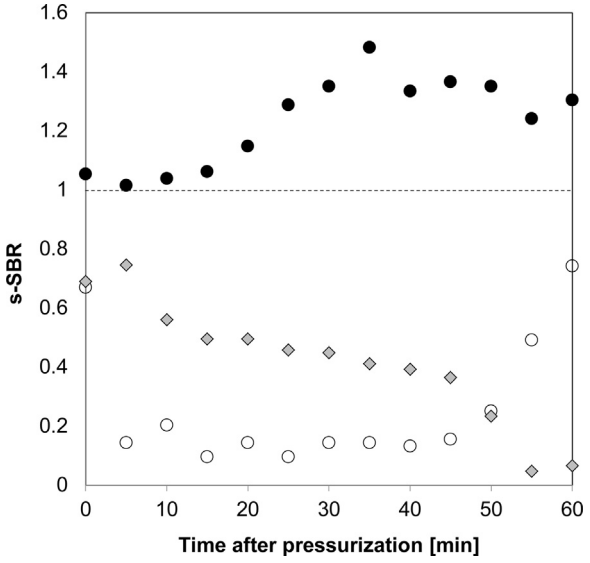

Fig. 6. s-SBR variation with various gases under P = 0.4 MPa condition during pressurizing period (II). Solid circles show s-SBR increasing after pressurization with normal air. Open circles show s-SBR decreasing after pressurization with air including 5% CO_2. Gray diamonds are those with N_2 gas. Dotted line shows Δ = 1, above which s-SBR is accelerated during the pressurizing period II. The inhibition effect Δ for these data is shown in Fig. 5.

where c_i is the gas concentration and D_i is the diffusion coefficient of component i in the medium. When P_i is large, the concentration gradient dc/dz is large, and so is the diffusion rate. Based on the above assumptions, the diffusion flux J_i of gas molecule i is

$$J_i = (D_i/\pi t)^{1/2} c_{0i}. \quad (3)$$

To compare the difference between Xe and O_2, we use the following values obtained in water

$$D_{Xe} = 1.54 \times 10^{-9}\ \mathrm{m^2/s}; c_{0Xe} = 7.88 \times 10^{-5},$$

$$D_{O2} = 2.04 \times 10^{-9}\ \mathrm{m^2/s}; c_{0O2} = 2.29 \times 10^{-5}.$$

D_i is estimated with the Wilke-Chang estimation method (Reid et al., 1987), and c_{0i} comes from the handbook (The Chemical Society of Japan, 2004), both being applied to the P, T conditions here. Using Eq. (3), both gases are expected to reach saturation at most 5 min after depressurization. This analysis suggests that sufficient Xe or O_2 reaches the network at the base of the MEA probe almost immediately after pressurization. As a result, the variation of s-SBR in Fig. 3 must be mainly controlled by factor (c), the reaction rate of Xe (or O_2) with the neuronal network.

We find that the decrease of s-SBR occurs soon after Xe pressurization. In fact, Fig. 3 shows that under Xe pressure, the time period required to become half of the final s-SBR is independent of P, being less than 10 min for all P conditions tested. This means that even a small amount of Xe can quickly inhibit the SB. This finding suggests that the active sites for Xe inhibition on a neuron are directly in contact with the medium, such as at a synaptic junction.

Xe pressure dependence on SB inhibition of neuronal network activity

The steady-state value of s-SBR under Xe pressure depends on P_{Xe} (see Fig. 3, dashed lines in period II). To help us examine the P_{Xe} dependence on Δ (Fig. 5), we fit this quantity with the Hill equation as follows:

$$\Delta = {P_{Xe}}^{\nu}/(k^{\nu} + {P_{Xe}}^{\nu}), \quad (4)$$

where k and ν are constants. As shown by the dotted line in Fig. 5, the curve fitting (Origin 9.1) gives k = 0.1 MPa and ν = 2.5 (R^2 = 0.994). From Henry's law, P_{Xe} linearly scales to the Xe concentration in the medium, C_{Xe}, and thus Eq. (4) shows the Xe concentration dependence on the SB inhibition in the neuronal network used in the present study.

Based on the k value, the effective concentration for the 50% SB inhibition is estimated to be when P_{Xe} = 0.1 MPa, which is equivalent to the Xe concentration of 0.5. However, the minimum alveolar concentration of Xe needed for rat anesthesia ranges between 0.64 and 0.71 (Goto et al., 1997). These values are equivalent to the effective concentration for the 90% SB inhibition (P_{Xe} = 0.22 MPa) on the obtained fitting curve, which corresponds to C_{Xe} = 9.5 mM.

As burst suppression in the electroencephalogram is an index of deep anesthesia, it is considered that more than 90% inhibition of SB is required for the anesthetic condition at the neuronal network level. Therefore, we suggest that the effective Xe concentration for sufficient inhibition of neuronal-network activities is above 9.5 mM in the medium.

The fitted value of $\nu = 2.5$ indicates that SB inhibition involves Xe reacting with two or three active sites of neuronal network. Our results cannot pinpoint the reaction sites of Xe; nevertheless, we speculate that dissolved Xe lowers the efficiency of signal transport at several synaptic junctions, and finally inhibits more than two connections per neuron. An increase in the number of synapses inhibited by Xe effectively divides the neuronal network into smaller sections. And if the neuronal network becomes smaller than the critical size (Ito et al., 2010), spontaneous SB in that network would stop. These ideas can explain the results obtained in the present study as follows: When the saturated Xe concentration is below 9.5 mM, SB partially stop, but the remaining network is larger than the critical size. Thus, the SBR remains, but at a level smaller than the control during the pressurization period. However, when the Xe concentration exceeds 9.5 mM, the divided sections of the network become smaller than the critical size, causing the SBR to decay to zero. The SBR then does not recover until enough Xe is removed from the neuronal network.

Influence of Xe-induced inhibition on the activity of frequently firing neurons

Our previous study (Uchida et al., 2012) indicated that the single spikes are independent of the Xe-induced SB inhibition. However, as Xe dissolves in the plasma membrane of neurons, thereby changing its properties (Booker and Sum, 2013; Uchida et al., 2015 Uchida et al., 2015), Xe might affect the firing activities of neurons. Here we examine the firing activities (*e.g.*, Fig. 2) in detail and describe several patterns of spike changes.

Under the normal condition, the total spike rate N_0 consists of the number of spikes in the bursts (N_b) and those in the single spikes (N_s):

$$N_0 = N_b + N_s. \tag{5}$$

In the mature neuronal network, N_0 usually nearly equals N_b because N_b is usually much larger than N_s (see Figs. 2 (I) and S1). This agrees with that found in Uchida et al. (2012). In a few channels among the 16 channels here, sparse single spikes occur in addition to the SBs (*e.g.*, channels #3, #4, #10, #14, and #15 in Fig. 2(I)).

Under complete inhibition of SBs, the total spike rate N_0 decreases drastically because N_b becomes zero (Uchida et al., 2012). The remaining number of spikes N_s' comes from the single spikes recorded in a few channels, which sometimes slightly differs from that in the control period N_s. This amount is defined as

$$N_s' = N_s - \Delta N_s + \Delta N_f, \tag{6}$$

where ΔN_s is the change in the single spike rate and ΔN_f is the additional spike rate by the frequent-firing neurons observed mainly under the Xe-induced SB inhibition conditions. The single spike rate sometimes slightly decreases (ΔN_s is positive in Eq. (6)) under the SB inhibition condition. For example, channels #3 and #4 in Fig. 2(I) become calm under Xe pressure (Fig. 2(II)) although channels #14 and #15 remain active. We consider that the effect of dissolved Xe in the plasma membrane would reduce the firing activity of some neurons. However, as we found earlier (Uchida et al., 2012), ΔN_s is usually negligible compared to N_s and N_b. So, we find again that the Xe dissolved in the plasma membrane is not the main cause of the SB inhibition. This also suggests that Xe does not affect the function of another type of intercellular connection in the neuronal network, a gap junction, which is considered to play a role on the synchronization in the network activities. Because ΔN_s is found to be small enough in the present study, the gap junction is also considered not to be inhibited significantly by Xe dissolved in the plasma membrane. Therefore, the main target of Xe for inhibiting SBs would be the synaptic junctions.

It is interesting, on the other hand, that we sometimes observed frequent-firing neurons in the network only during the SB inhibition (*e.g.*, channels #7 and #8 in Fig. 2(II)). Such neurons are not easy to detect under the control condition (Fig. 2(I)), but noticeable during complete SB inhibition. The appearance of the frequent-firing neurons under Xe pressure is considered as follows. The frequent-firing neuron is considered to have a relatively high membrane potential and thus easily fires (*e.g.*, (Zbinden, 2011)). In the mature neuronal network, SBs occur frequently ($N_0 \sim 10^4$ cpm), thus the membrane potential in a given neuron would be suppressed a little lower, which depresses the frequent firing under the control condition. However, when the SBs are inhibited by Xe, N_0 decreases to about a fifth (see Fig. S1 and Fig. 7 in Uchida et al., 2012), thus the membrane potential of the neuron would be as high as its original value due to the small number of spikes. In this way, the frequent-firing neurons become active. After the Xe concentration in the system decreases and the SB recovers (Fig. 2(III)), these frequent-firing neurons become calm again. This is caused by a lowering of their membrane potential due to the frequent SBs occurring in the system again.

Although the role of the frequent-firing neurons on the neuronal network activities has not been revealed yet, it might have important roles such as being the leading (initial firing) neuron, or it has hub connections in the active neuronal network. To study about the frequent-firing neurons, the temporal control of neuronal network activities with gas application would be one promising way.

Possible effect of oxygen on the neuronal network activities

Besides the Xe-induced inhibition effects on SBs, we found a slight acceleration effect ($\Delta > 1$) when a low P_{Xe} (<0.1 MPa) mixed gas was applied at high P to the neuronal network (see Figs. 5 a–d and S2a–d). In these experiments, the partial pressure of O_2 increased in proportion to the increase in total pressure. The comparative experiments with N_2 gas and with normal air containing 5% CO_2 at $P = 0.4$ MPa with a fixed partial pressure of O_2 showed no such acceleration effect. This result indicates that the apparent acceleration effect is from the O_2 enriched in the medium under pressurization conditions.

The effect of O_2 on the burst activities of neuronal networks has previously been studied mainly for the hypoxia (low O_2 concentration) condition. Using an electroencephalogram, one study found that a rat brain became isoelectric when hypoxic (Rabinorici et al., 2000). Moreover, according to Wilson et al. (2003), the burst activity of the spinal cord of neonatal mouse decreases under hypoxia (equilibrated with 5% O_2 + 5% CO_2 + 90% N_2) at atmospheric pressure, which is equivalent to $P_{O2} = 5$ kPa. The burst activity recovers under hyperoxia (equilibrated with 95% O_2 + 5% CO_2) at the same atmospheric pressure. As all experiments here included at least 0.1 MPa normal air, which was air from a room well-ventilated with outside air. As a result, P_{O2} was about 21 kPa or more, which is an O_2 amount much larger than the hypoxia conditions. Thus, we may be seeing a similar effect, but at higher pressure.

In contrast, when we added Xe in the previously discussed experiments, we did not decrease (or increase) P_{O2}, and thus the observed Xe inhibition effect on SBs could not have been influenced by changes in P_{O2}. Nevertheless, the present study indicates the possibility of an acceleration effect of O_2 on the burst activities at the neuronal network level. These experiments do not give a quantitative measure of the acceleration effect, but suggest that fur-

ther experiments may reveal the hyperoxia effect on the neuronal network activities.

Conclusions

We observed the electrical activities of neonatal rat cortical neuronal networks on an MEA under air–Xe mixtures, focusing on spontaneous synchronized bursts. These bursts were found to be specifically and reversely inhibited by the dissolved Xe. When the partial Xe pressure increased, the synchronized burst rate decreased in good agreement with the Hill equation. Assuming that a deep anesthetic effect requires more than 90% inhibition of activities in the neuronal network level, we argued that the threshold concentration of Xe in the medium is about 9.5 mM for deep anesthesia. This concentration is consistent with our previous findings (Uchida et al., 2012). The results indicated that Xe-induced inhibition of synchronized bursts is mainly due to the segmentation of the network into a size smaller than the critical size (Ito et al., 2010) by a relatively random inhibition of the connections between neurons. The occurrence of frequent-firing neurons in the network was found to increase during the synchronized burst inhibition with Xe pressurization. This indicates that Xe inhibits the synchronization between neurons, not the firing activity of the neurons. We also found indications that a hyperoxia condition can accelerate the network activities when the Xe-inhibition effect is small ($P_{Xe} < 0.1$ MPa).

Acknowledgments

This work was partly supported financially by a Grant-in-Aid for Scientific Research from the Japan Society for the Promotion of Science (grant numbers 17340125, 23350001, 17K18834 and 26105009). The experimental data have also been accumulated by Mrs. Shotaro Suzuki, Yudai Hirano, and Kota Kume. We thank Professor Amadeu K. Sum for his fruitful discussion on gas molecule behaviors in solution. We also acknowledge Dr. Jon Nelson for his proofreading and valuable comments and suggestions that improved the manuscript.

Appendix A. Supplementary data

Supplementary data associated with this article can be found, in the online version, at http://dx.doi.org/10.1016/j.ibror.2017.09.001.

References

Banno, M., Mizuno, T., Kato, H., Zhang, G., Kawanokuchi, J., Wang, J., Kuno, R., Jin, S., Takeuchi, H., Suzumura, A., 2005. The radical scavenger edaravone prevents oxidative neurotoxicity induced by peroxynitrite and activated microglia. Neuropharmacology 48, 283–290.

Booker, R.D., Sum, A.K., 2013. Biophysical changes induced by Xenon on phospholipid bilayers. Biochim. Biophys. Acta 1828, 1347–1356.

Cullen, S.C., Gross, E.G., 1951. The anesthetic properties of xenon in animals and human beings, with additional observations on krypton. Science 113, 580–582.

Dawe, R.A., Miller, K.W., Smith, E.B., 1964. Solubility relations of fluorine compounds and inert gas narcosis. Nature 204, 789.

de Sousa, S.L.M., Dickinson, R., Lieb, W.R., Franks, N.P., 2000. Contrasting synaptic actions of the inhalational general anesthetics isoflurane and xenon. Anesthesiology 92, 1055–1066.

Dickinson, R., Peterson, B.K., Banks, P., Simills, C., 2007. Competitive inhibition at the glycine site of the N-methyl-D-aspartate receptor by the anesthetics xenon and isoflurane. Evidence from molecular modeling and electrophysiology. Anesthesiology 107, 756–767.

Dinse, A., Fohr, K.J., Georgieff, M., Beyer, C., Bulling, A., Weight, H.U., 2005. Xenon reduces glutamate-, AMPA-, and kainite-induced membrane currents in cortical neurons. Br. J. Anaesth. 94, 479–485.

Dorsch, R.R., Distefano, V., 1973. A generalized hydrate mechanism for gaseous anesthesia: Part II. Exp. Physiol. Chem. Phys. 5, 225–236.

Dorsch, R.R., deRocco, A.G., 1973. A generalized hydrate mechanism for gaseous anesthesia: Part I. Theory Physiol. Chem. Phys 5, 209–223.

Dorsch, R.R., 1970. Intermolecular Forces, Gas Hydrates and Gaseous Anesthesia. Phd Thesis. Faculty of the Graduate School of the Univ. Maryland, p. 157.

Eger II, E.I., Liao, M., Laster, M.J., Won, A., Popovich, J., Raines, D.E., Solt, K., Dutton, R.C., Cobos II, F.V., Sonner, J.M., 2006. Contrasting roles of the n-methyl-d-aspartate receptor in the production of immobilization by conventional and aromatic anesthetics. Anesth. Analg. 102, 1397–1406.

Eger, E., Raines, D., Shafer, S., Hemmings, H., Sonner, J., 2008. Is a new paradigm needed to explain how inhaled anesthetics produce immobility? Anesth. Analg. 107, 832–848.

Evers, A.S., Berkowitz, B.A., d'Avignon, D.A., 1987. Correlation between the anesthetic effect of halothane and saturable binding in brain. Nature 328, 157–160.

Franks, N.P., Lieb, W.R., 1994. Molecular and cellular mechanisms of general anesthesia. Nature 367, 607–614.

Franks, N.P., Dickinson, R., de Sousa, S.L.M., Hall, A.C., Lieb, W.R., 1998. How does xenon produce anaesthesia? Nature 396, 324.

Georgiev, S.K., Furue, H., Baba, H., Kohno, T., 2010. Xenon inhibits excitatory but not inhibitory transmission in rat spinal cord dorsal horn neurons. Mol. Pain 6, 25.

Goto, T., Saito, H., Nakata, Y., Uezono, S., Ichinose, F., Morita, S., 1997. Emergence times from xenon anaesthesia are independent of the duration of anaesthesia. Br. J. Anaesth. 79, 595–599.

Gruss, M., Bushell, T.J., Bright, D.P., Lieb, W.R., Mathie, A., Franks, N.P., 2004. Two-pore-domain K+ channels are a novel target for the anesthetic gases xenon, nitrous oxide, and cyclopropane. Mol. Pharmacol. 65, 443–452.

Haseneder, R., Kratzer, S., Kochs, E., Eckle, V.-S., Zieglgansberger, W., Rammes, G., 2008. Xenon reduces N-methyl-D-aspartate and –amino-3-hydroxy-5-methyl-4-isoxazolepropionic acid receptor mediated synaptic transmission in the amygdala. Anesthesiology 109, 998–1006.

Hirota, K., Sasaki, R., 2011. Electrophysiological approach to mechanisms for actions of general anesthetics. Masui (Jpn. J. Anesthesiol.) 60, 574–581 (in Japanese with English abstract).

Honma, S., Shirakawa, T., Katsuno, Y., Namihira, M., Honma, K., 1998. Circadian periods of single suprachiasmatic neurons in rats. Neurosci. Lett. 250, 157–160.

Hosokawa, C., Kudoh, S.N., Kiyohara, A., Taguchi, T., 2008. Resynchronization in neuronal network divided by femtosecond laser processing. Neuroreport 19, 771–775.

Ito, D., Tamate, H., Nagayama, M., Uchida, T., Kudoh, S.N., Gohara, K., 2010. Minimum neuron density for synchronized bursts in a rat cortical culture on multi-electrode arrays. Neuroscience 171, 50–61.

Ito, D., Komatsu, T., Gohara, K., 2013. Measurement of saturation processes in glutamatergic and GABAergic synapse densities during long-term development of cultured rat cortical networks. Brain Res. 1534, 22–32.

Kaisti, K.K., Långsjö, J., Aalto, S., Oikonen, V., Sipilä, H., Teräs, M., Hinkka, S., Metsähonkala, L., Scheinin, H., 2003. Effects of sevoflurane, propofol, and adjunct nitrous oxide on regional cerebral blood flow, oxygen consumption, and blood volume in humans. Anesthesiology 99, 603–613.

Kudoh, S.N., Hosokawa, C., Kiyohara, A., Taguchi, T., Hayashi, I., 2007. Biomodeling system – interaction between living neuronal networks and the other world. J. Robot. Mech. 19, 592–600.

Laitio, R., Kaisti, K., Långsjö, J., Aalto, S., Salmi, E., Maksimow, A., Aantaa, R., Oikonen, V., Sipilä, H., Parkkola, R., Scheinin, H., 2007. Effects of xenon anesthesia on cerebral blood flow in humans: a positron emission tomography study. Anesthesiology 106, 1128–1133.

Laitio, R., Långsjö, J., Aalto, S., Kaisti, K., Salmi, E., Maksimow, A., Aantaa, R., Oikonen, V., Viljanen, T., Parkkola, R., Scheinin, H., 2009. The effects of xenon anesthesia on the relationship between cerebral glucose metabolism and blood flow in healthy subjects: a positron emission tomography study. Anesth. Analg. 108, 593–600.

Lawrence, J.H., Loomis, W.F., Tobias, C.A., Turpin, F.H., 1946. Preliminary observations on the narcotic effect of xenon with a review of values for solubilities of gases in water and oils. J. Physiol. 105, 197–204.

Liu, L., Xu, Y., Tang, P., 2010. Mechanistic insights into xenon inhibition of NMDA receptors from MD simulations. J. Phys. Chem. B 114, 9010–9016.

Ma, D., Wilhelm, S., Maze, M., Franks, N.P., 2002. Neuroprotective and neurotoxic properties of the 'inert' gas, xenon. Br. J. Anesth. 89, 739–746.

Matsumoto, J., 1995. Molecular mechanism of biological responses to homoeopathic medicines. Med. Hypotheses 45, 292–296.

Mayer, K.H., 1937. Contributions to the theory of narcosis. Trans. Faraday Soc. 33, 1062–1069.

Meyer, H., 1899. Zur theorie der alkoholnarkose. Naunyn-Schmiedebergs Arch. Pharmakol. 42, 109–118.

Miller, S.L., 1961. A theory of gaseous anesthetics. Proc. Natl. Acad. Sci. 47, 1515–1524.

Miller, K.W., 1969. How do anesthetics work? Anesthesiology 30, 127–128.

Nakahiro, M., Yeh, J.Z., Brunner, E., Narahashi, T., 1989. General anesthetics modulate GABA receptor channel complex in rat dorsal root ganglion neurons. FASEB J. 3, 1850–1854.

Negale, P., Metz, L.B., Crowder, C.M., 2005. Xenon acts by inhibition of non-N-methyl-D-aspartate receptor-mediated glutamatergic neurotransmission in caenrhabditis elegans. Anesthesiology 103, 508–513.

Overton, E., 1901. Studien über die Narkose: Zugleich ein Beitrag zur Allgemeinen Pharmakologie. Verlag von Gustav Fischer, JENA, pp. 195.

Pauling, L., 1961. A molecular theory of general anesthesia. Science 134, 15–21.

Preckel, B., Schlack, W., 2005. Inert gases as the future inhalational anaesthetics? Best Pract. Res. Clin. Anaesthetiol. 19, 365–379.

Rabinorici, G.D., Lukatch, H.S., MacIver, M.B., 2000. Hypoglycemic and hypoxic modulation of cortical micro-EEG activity in rat brain slices. Clin. Neurophysiol. 111, 112–121.
Reid, R.C., Prausnitz, J.M., Poling, B.E., 1987. The properties of gases and liquids, 4th edn. McGraw-Hill, New York, pp. 598–599.
Rex, S., Schaefer, W., Meyer, P., Rossaint, R., Boy, C., Setani, K., Büll, U., Baumert, J., 2006. Positron emission tomography study of regional cerebral metabolism during general anesthesia with xenon in humans. Anesthesiology 105, 936–943.
Salmi, E., Laitio, R.M., Aalto, S., Maksimow, A.T., Långsjö, J.W., Kaisti, K.K., Aantaa, R., Oikonen, V., Metsähonkala, L., Någren, K., Korpi, E.R., Scheinin, H., 2008. Xenon does not affect gamma-aminobutyric acid type a receptor binding in humans. Anesth. Analg. 106, 129–134.
Schoenborn, B.P., Featherstone, R.M., Vogelhut, P.O., Susskind, C., 1964. Influence of xenon on protein hydration as measured by a microwave absorption technique. Nature 202, 695–696.
Stedman's Medical Dictionary, 2006. Stedman's Medical Dictionary, 28th ed. Lippincott, Williams, & Wilkins, Philadelphia.
Takeuchi, H., Mizuno, T., Zhang, G., Wang, J., Kawanokuchi, J., Kuno, R., Suzumura, A., 2005. Neuritic beading induced by activated microglia is an early feature of neuronal dysfunction toward neuronal death by inhibition of mitochondrial respiration and axonal transport. J. Biol. Chem. 280, 10444–10454.
The Chemical Society of Japan, 2004. Kagaku-binran (Handbook of chemistry), 5th edn. Maruzen Co. Ltd., Tokyo, fundamental II-145–146.
Uchida, T., Suzuki, S., Hirano, Y., Ito, D., Nagayama, M., Gohara, K., 2012. Xenon-induced inhibition of synchronized bursts in a rat cortical neuronal network. Neuroscience 214, 149–158.
Uchida, T., Nagayama, M., Yamazaki, K., Gohara, K., Sum, A.K., 2015. Raman spectra measurements on DEPC liposome and cell membrane of living neuron under xenon pressure. Can. J. Chem. 93, 831–838.
Wilson, R.J.A., Chersa, T., Whelan, P.J., 2003. Tissue PO_2 and the effects of hypoxia on the generation of locomotor-like activity in the in vitro spinal cord of the neonatal mouse. Neuroscience 117, 183–196.
Wilson, N.R., Ty, M.T., Ingber, D.E., Sur, M., Liu, G., 2007. Synaptic reorganization in scaled networks of controlled size. J. Neurosci. 27, 13581–13589.
Yamakura, T., Harris, R.A., 2000. Effects of gaseous anesthetics nitrous oxide and xenon on ligand-gated ion channels: comparison with isoflurane and ethanol. Anesthesiology 93, 1095–1101.
Zbinden, C., 2011. Leader neurons in leaky integrate and fire neural network simulations. J. Comput. Neurosci. 31, 285–304.